# CERN Summer Studentship 2023

## iRPC studies based on Backend-electronics

Shima Osloub

**from 26/6/2023 to 18/8/2023**

**Supervisor:** Prof. Salvatore Buontempo

**Abstract**

This study begins with a brief overview of the data acquisition system of iRPC (improved Resistive Plate Chambers) and the data analysis procedure. Two main projects are discussed which are data analysis to find the gap spacer structure from random trigger data with gamma-ray source in GIF++ and the second project is obtaining the efficiency of the newly assembled chamber with cosmic rays. The results are presented in project sections and conclusions are discussed in each section.

# Contents

**1 Introduction** **1**

1.1 Motivation for iRPCs . . . . . . . . . . . . . . . . . . . . . . . . . . . . . . . . . . 3

1.2 Back-End Electronics (BEE) and Front-End Electronics (FEE) of iRPCs . . . . . . . 3

1.3 Data Acquisition (DAQ) and Data Analysis . . . . . . . . . . . . . . . . . . . . . . . 4

**2 First project: Data analysis with gamma source** **6**

**3 Second Project: Efficiency analysis with cosmics** **10**

**4 References** **14**

# List of Figures

1 A quadrant of the CMS experiment. The red box indicates the region where iRPCs (RE3/1 and RE4/1) will be placed to extend the muon coverage. . . . . . . . . . . . 2

2 A Schematic view of how the double gap RPCs detect muon in CMS . . . . . . . . . 3

3 Illustration of how the iRPC measures the position of muon along the strip . . . . . 4

4 Detector data frames of Uplink data format from FE to BE . . . . . . . . . . . . . . 5

5 Schematic of reading data based on the trigger signal . . . . . . . . . . . . . . . . . . 5

6 Schematic view of data analysis . . . . . . . . . . . . . . . . . . . . . . . . . . . . . . 6

7 Plots of data analysis of one strip with different bin widths (0.5/0.9/1.5/2cm) . . . 7

8 Picture of strips with the position of spacers . . . . . . . . . . . . . . . . . . . . . . . 7

9 Plots of data analysis for finding the position of spacers for each strip . . . . . . . . 8

10 Gamma hit distribution for both gaps . . . . . . . . . . . . . . . . . . . . . . . . . . 9

11 Using a lead brick in order to see the affection in data and plots. . . . . . . . . . . . 9

12 Plots of each strip that are affected and not affected by the lead brick . . . . . . . . 10

13 A schematic view of cosmic setup and data acquisition . . . . . . . . . . . . . . . . . 10

14 Cosmic setup at building 904 . . . . . . . . . . . . . . . . . . . . . . . . . . . . . . . 11

15 Histogram of the hit count of the events for each strip . . . . . . . . . . . . . . . . . 11

16 Hit map of the event detected by the half chamber . . . . . . . . . . . . . . . . . . . 12

17 Efficiency curve of QC test of newly assembled chamber . . . . . . . . . . . . . . . . 13

# 1 Introduction

The Large Hadron Collider (LHC) is the world's largest and most powerful particle accelerator. CMS (compact muon solenoid) is one of the LHC experiments located at CERN between the French and Swiss border and CMS is mostly used for studying muons and beyond standard model particles. In order to extend the sensitivity for searching beyond standard model particles, the LHC will be improved by higher luminosity (HL-LHC). The LHC will be improved during the Long Shotdown3 (LS3) and the HL-LHC upgrade run would start in 2026 and end in 2038. This improvement will be beneficial for searching for new beyond standard model particles like supersymmetry and new heavy gauge bosons. Also, the accuracy for standard model tests will be improved, because by increasing the luminosity, the center of mass energy of protons will be 14 TeV and the integrated luminosity gets to 3000 fb$^{-1}$ and this higher luminosity increases the collision rates by a factor of 5. The main challenge for the detection of particles in HL-LHC is the high rate of production of

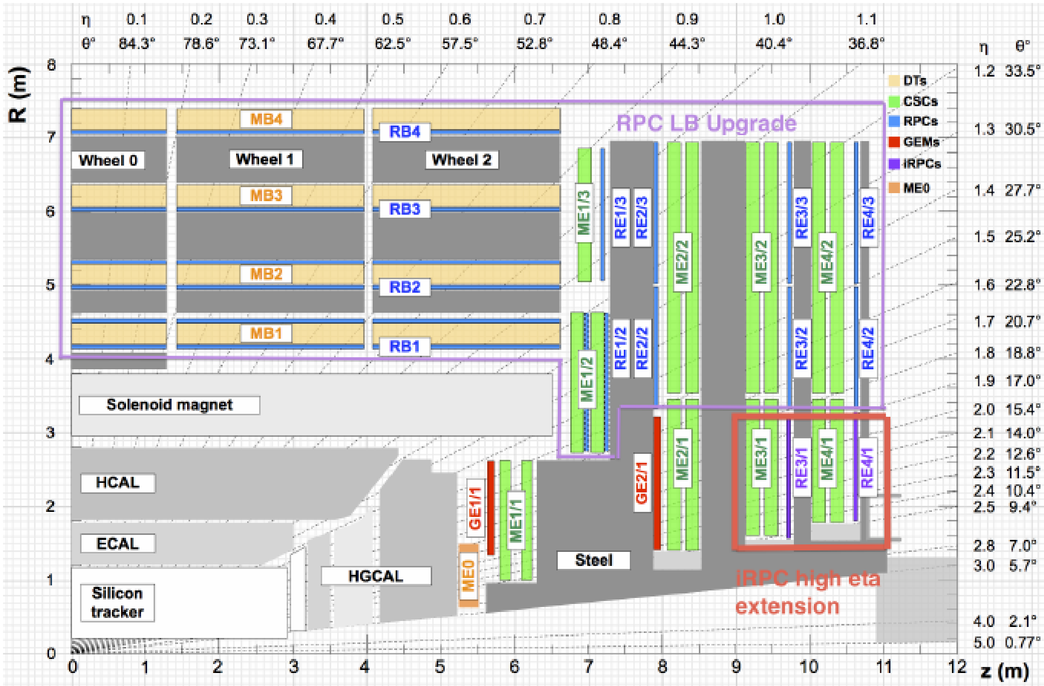


Figure 1: A quadrant of the CMS experiment. The red box indicates the region where iRPCs (RE3/1 and RE4/1) will be placed to extend the muon coverage.

particles, 100 proton-proton interaction for every bunch crossing taking place every 25 ns yielding billions of secondary particles each second.

One of the most important particles that CMS detects is muons. The muon detectors play a central role in CMS. Muon can be identified and measured individually and accurately because their lifetime is big enough to be detected separately in muon detectors and also, they stand out from the large hadronic background. CMS was built with several complementary subdetectors to identify muons, already at trigger level and to measure their momentum and charge over a broad range of kinematics.

Muon detection experiments at the forward region are particularly challenging because at high pseudorapidity ($|\eta| = 4$) the background is at its maximum rate, which makes it difficult to study light particles. Also, it includes high rate of produced particles, therefore we need new electronics with deeper buffering for data acquisition. Another challenge related to the large background is the event reconstructions for these large numbers of particles so there would be needed very good spatial and time resolution. Most backgrounds and most muons are produced in the forward direction at high pseudorapidity, so it is also needed muon chambers in the forward region. For this reason, there are different kinds of detectors in CMS as it is shown in Figure 1, a quadrant of the CMS experiment. One of these kinds of detectors is RPC.

The RPCs are double-gap chambers operated in avalanche mode, at the high electric field. They use High-Pressure Laminate (HPL, commonly known as Bakelite) electrodes with a high bulk resistivity. RPCs are mainly used for accurate timing and fast triggering, with an excellent intrinsic resolution of about 1.5 ns for a double-gap chamber, the schematic layout is illustrated in Figure 2. The present RPC system consists of 480 chambers in the barrel and 576 chambers in the endcap, organized in 4 stations called RB1 to RB4 in the barrel region, and RE1 to RE2 in the endcap region.

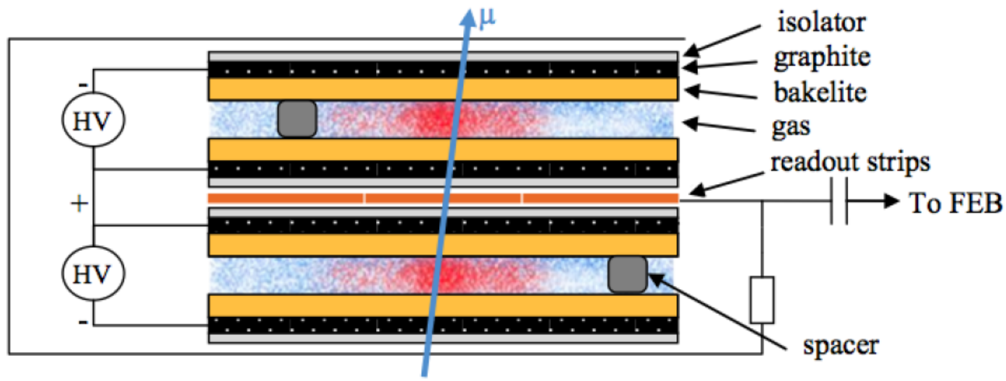


Figure 2: A Schematic view of how the double gap RPCs detect muon in CMS

For the HL-LHC more detectors are needed in the forward region with higher accuracy. Thus, iRPCs can be used at HL-LHC. The red box in Figure 1 indicates the region where iRPCs will be placed to extend the muon coverage.

### 1.1 Motivation for iRPCs

The reasons for complementing the RPC with iRPCs in the forward system with the RE3/1 and RE4/1 chambers are that the new improved RPC type (iRPCs) are able to cope with the HL-LHC rates. Thus RE3/1 and RE4/1 complement the CMS forward muon system following the original plans. Also, the intrinsic time resolution is improved by about a factor of just over two for the measurements of RE3/1 and RE4/1. This improves background hit rejection and identification and reconstruction of slowly moving heavy stable charged particles. In addition, the new iRPCs will feature a better spatial resolution of the order of a few cm along the strip direction, by measuring the time difference between the signals at both ends of the readout strips. This helps in resolving ambiguities in the endcap trigger for multiple tracks.

The reason that iRPCs are used in the new stations RE3/1 and RE4/1 for Phase-2, is to sustain the high expected rates of up to 2 kHz/cm$^2$ with a hit efficiency well above 95 percent and the redundancy will be increased in the difficult endcap region. Moreover, iRPCs use thinner electrodes and a narrower gas gap, both reduced from a thickness of 2mm in the current design to 1.4mm which improves the detection of muons.

### 1.2 Back-End Electronics (BEE) and Front-End Electronics (FEE) of iRPCs

The new iRPC chambers are conceived such that the amount of deposited charge associated with the passage of charged particles is reduced with respect to the present CMS RPCs. In order to detect the lower charges without affecting the detector performance, it is not possible to operate with the same Front-End Board (FEB) developed for the present system. A new FEB equipped with low-noise FEE based on the latest available technology, and a new off-detector DAQ system are developed.

The FEE has to be able to detect signals with a charge as low as 10 fC and needs also to be fast and reliable, and it must sustain the high irradiation environment that will prevail in RE3/1 and RE4/1 during the HL-LHC phase. The latest available technologies that minimize the chip size are proposed, so the new low-noise FEE, the corresponding ASIC, the CMS RPCROC, is developed to the needs of CMS.

Because of the same reason, the new BEE should be developed for iRPCs. The final system of BEE is constructed based on the Advanced Telecom Computing Architecture standard and will be installed for the system running. iRPC back-end board (BEB) has the functionalities of integration of fast and slow control, data reception, processing, and readout. The functional architecture of the BEB developed is that each BEB can handle inputs from multiple FEBs independently. The BEB buffers the data frames received from FEB via the GBT link, performs cross-clock processing, and disassembles them into GBT SC and user data. Whether it is a TDC data or a FEE SC answer is determined from the FEB for user data. More information about this section can be found in Refs. [1,2].

### 1.3 Data Acquisition (DAQ) and Data Analysis

In iRPCs, the new chambers are read out by a large trapezoidal printed circuit readout board which contains 96 strips, therefore, there are 192 channels per chamber. Each strip will be read from both sides with two channels. Each channel provides a time measurement that is sent to the DAQ system, so that DAQ system can determine the coordinate along the strip by a measurement of the difference in arrival time of the two signals which is shown in Figure 3.

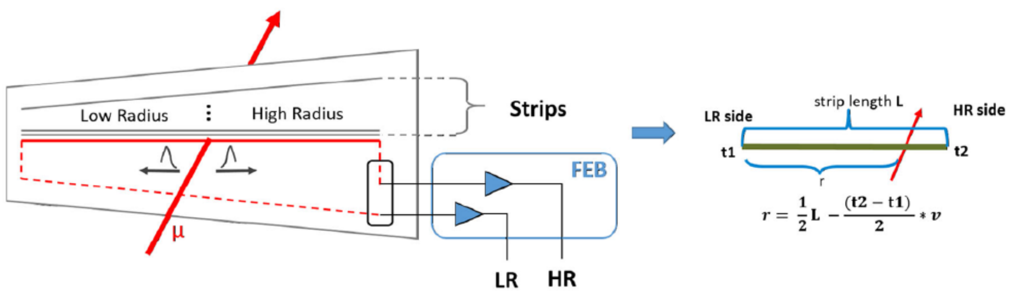


Figure 3: Illustration of how the iRPC measures the position of muon along the strip

Here in Figure 3, t1 is the arrival time on one strip end and t2 is that associated with the other one. v is the signal propagation velocity and L is the total strip length. The resolution of r is estimated and found to be about 1.7 cm.

The FEE of the iRPCs is a 32-channel ASIC using a broadband fast pre-amplifier and a fast discriminator. Its overall bandwidth is 1 GHz with a gain of 25. Each channel provides a charge measurement and a trigger output that can be used to measure the signal arrival time. The ASICs is hosted on the FEB that is attached to the RPC detector. On the same board, it is also present an FPGA device running a TDC for time measurement. To connect the strip's ends to an ASIC channel a coaxial cable with the same strip impedance is used. FEE has an excellent timing resolution of about 11-20 ps, resulting in a positional resolution of about 1.7 cm along the strip. For iRPC the system configuration and time measurement of the FEE rely on the fast and slow control (SC) provided by the BEE. The high-precision time information of the iRPC system requires high synchronization of each part and real-time transmission. Therefore, the information interaction between the front-end (FE) and back-end (BE) includes fast control signals (time reference, etc.), SC commands (parameter configuration, etc.), and data (time information, etc.). The 4.8 Gbps GBT link is selected to realize the point-to-point connection between the FEE and BEE.

The FEB and BEB are connected by Uplink and Downlink, a bidirectional fiber, which uplink is used to send data from FEB to BEB and downlink sends commands and control information from BEB to FEB. The uplink from the FE to the BE adopts the Wide Bus Frame mode with higher bandwidth since the FEE is located in an intense radiation environment. The downlink from the BE to the FE adopts the GBT Frame mode with an error correction function. An uplink frame has a 16 bits header dedicated to the fast status. These bits allow monitoring of the state of the three FPGAs. Moreover, in this header, there are a few bits reserved to identify if this is either data or control (or nothing) in the payload. The following Figure 4 shows the generic data frame format for single-channel data.

| *Data frame* | Header (status flags) | | | | | | | TDC Data Standard Payload | | | | | | | | |
|---|---|---|---|---|---|---|---|---|---|---|---|---|---|---|---|---|
| *Fied Name* | Resync LB | BC0 LB | MiscStatus | SCFrame | IsStrip | RSVD | DataValid | devAddr | chanID | TDC data | devAddr | chanID | TDC data | devAddr | chanID | TDC data |
| *Field length* | 1 | 1 | 7 | 1 | 2 | 1 | 3 | 2 | 6 | 24 | 2 | 6 | 24 | 2 | 6 | 24 |
| *GBT Frame Group* | G4 | | | | | | | G3 & G2 | | | G1 & G0 | | | G6 & G5 | | |

Figure 4: Detector data frames of Uplink data format from FE to BE

In this mode, a given piece of data is 32 bits wide and is related to only 1 TDC-generated timestamp. The uplink user data (112 bits) carries three types of information: fast control status, response to SC read requests, and collected detector data (i.e., “TDC data”), Each frame is allowed to transmit up to 3 TDC data, and the TDC data is composed of an 8-bit position and 24-bit time information.

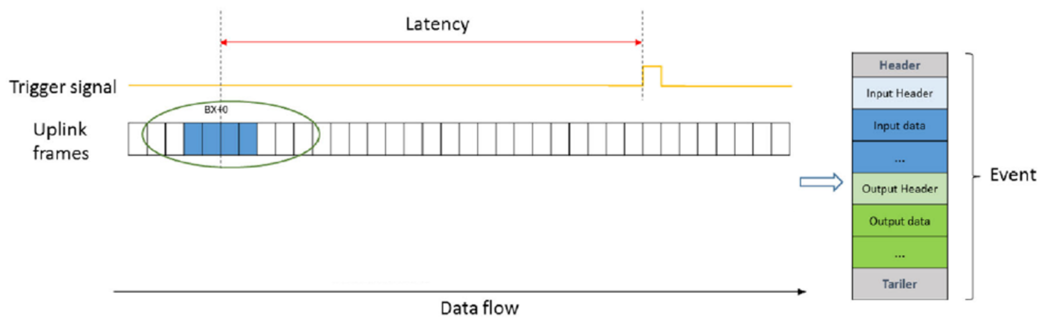


Figure 5: Schematic of reading data based on the trigger signal

Due to the limited transmission bandwidth, the TDC data collected by the FEE at the same bunch crossing (BX), requires multiple uplink frames to be completely sent to the BEE. The DeMux algorithm is used to recover the time relationship of the received TDC data to the time of generation on the BX scale. FEE is based on data-driven output, that is continuous output as long as the signal is collected. Therefore, BEE must receive and process in real-time, recovering the time relationship between incoming detector data. BEE then converts the detector data into the fired strips’ position and time information and clusters these individual hits. Under the premise of this calibration of the latency between the trigger signal and data, BEE selects raw detector data and TPs (trigger primitives) based on the trigger signal, packs, and sends these data to the DAQ system according to the specified data format. This mechanism means that only relevant data regarding events of interest will be read out. The BEE distributes the clock and BC0 signal to the FEE via the downlink, so, the FE and BE will have the same time reference. The difference between the bunch crossing number (BCN) of the BEB and the timestamp carried by the TDC data is the delay between the transmission and generation of TDC data which is shown schematically in Figure 5.

The BEE must read out the raw detector data, the TDC data received by the BE Based on the

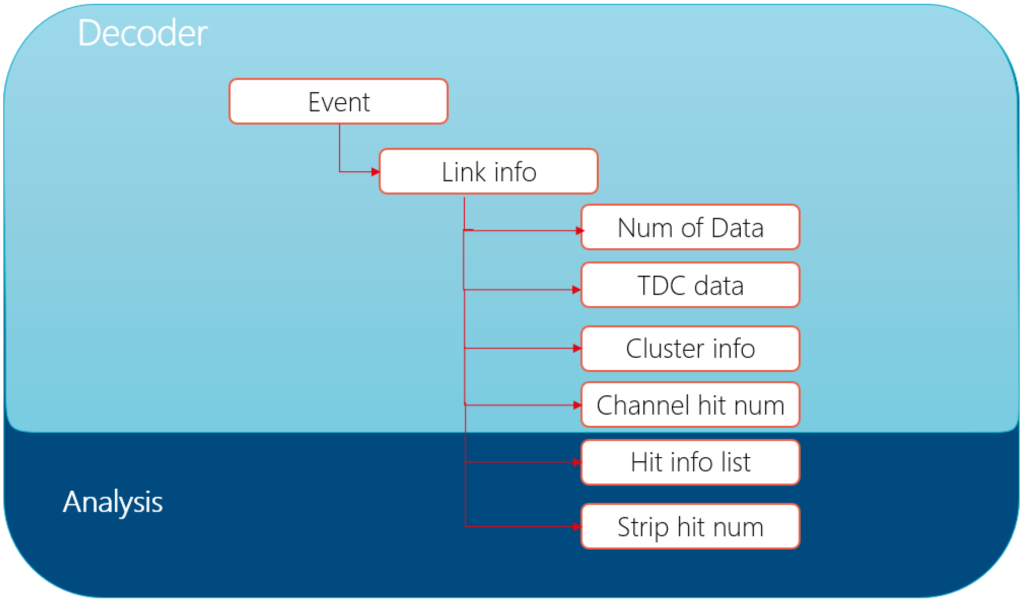


Figure 6: Schematic view of data analysis

pipeline design, as long as the latency between the trigger signal and the data is known, the latency value can be converted into the address offset of the buffer to read out the data related to the trigger signal directly. The time spent by the BEE from receiving the uplink frame carrying "TDC data" to give the TPs is fixed, so it is only necessary to calibrate the time relationship between the trigger signal and the TDC data. As shown in Figure 5, after calibrating the latency between the trigger signal and the data, read the TDC data input from the FE and the TPs output from the BE in a certain window, package the data of multiple links, and assemble them into an event, and then upload the event to the DAQ system.

After the transmission of these data to the PC a decoder script will analyze the data and give us the information we need. This decoder script first reads and checks the format of the data and sends it to the link info class which includes functions that can read the information that we need from data including the number of events, TDC data, channel hit number, cluster information, etc, and the functions of hit information list and strip hit numbers can do the analysis. The process is shown in summary in Figure 6.

## 2 First project: Data analysis with gamma source

This project was proposed by Prof. Iuri Bagaturia and the aim of that project is to use the hit profile of the chamber to see if we can get the clear spacers' positions for the half chamber. We expect that there should be "dips" of reduced trigger efficiency because the signals that are detected by chambers are from the avalanche that happens inside the gap, so the spacers can be regarded as dead areas as it was shown in Figure 2, two plates are glued together with the spacer mesh on the inside to form the basic chamber. For this purpose, we analyze the data of new chambers with new electronics by gamma-ray source (without beam) and with the random trigger in GIF++.

We used RE4/1 and RE3/1 chambers for these tests and the random trigger frequency was 2kHz. The Gamma source attenuation coefficient was 3.3 and the order of typical total events

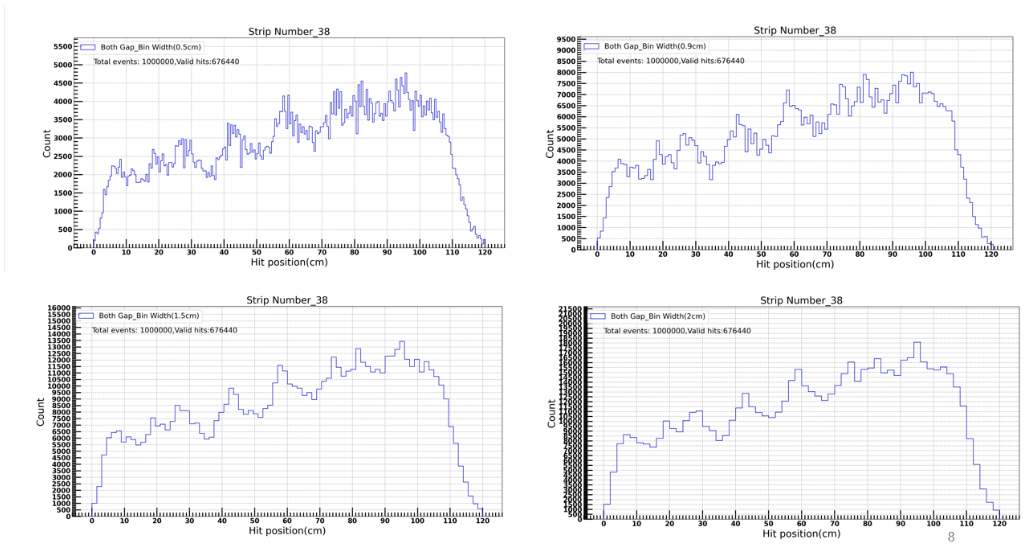


Figure 7: Plots of data analysis of one strip with different bin widths (0.5/0.9/1.5/2cm)

statistic was about 0.7-1$\times 10^6$ events. We did this Measurement in different modes: putting high voltage to both gaps or only single gap. For the single gap mode, we should see the effects of spacers on each strip, but for both gaps, since the spacers for two gaps are shifted, we should see a nearly uniform distribution.

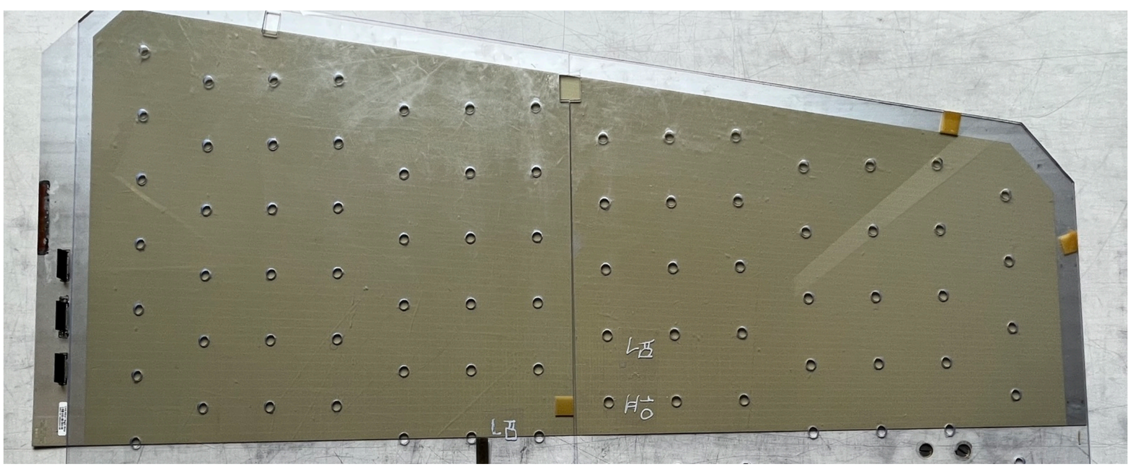

Figure 8: Picture of strips with the position of spacers

We did this data analysis and made histogram plots for different bin widths to find out that which bin width would be better for finding the spacer effects and we expect that to be around 0.8 cm due to the fact that the diameter of the spacers is around 0.8cm. It is shown in Figure 7, that for different bin widths, we have gotten the same distribution which shows that our measurement is robust and the number of total events is enough to see the expected distribution.

We have done the analysis for each strip with each gap and both gaps in order to see the effect of spacers on each strip. The positions of the spacers and the strips are shown in Figure 8, and we got the resulting plots like Figure 9. For each spacer, we should see a dip in the distribution at the spacer's position, but the number of dips in our plots is not the same as the number of spacers that affect each strip. For example, from Figure 8 we can see that strip number 1, which is at the lowest part of the picture, would be affected by 7 spacers, and strip number 38 is not affected by any spacers. However, in Figure 8 we cannot see the effects of these spacers on the strips.

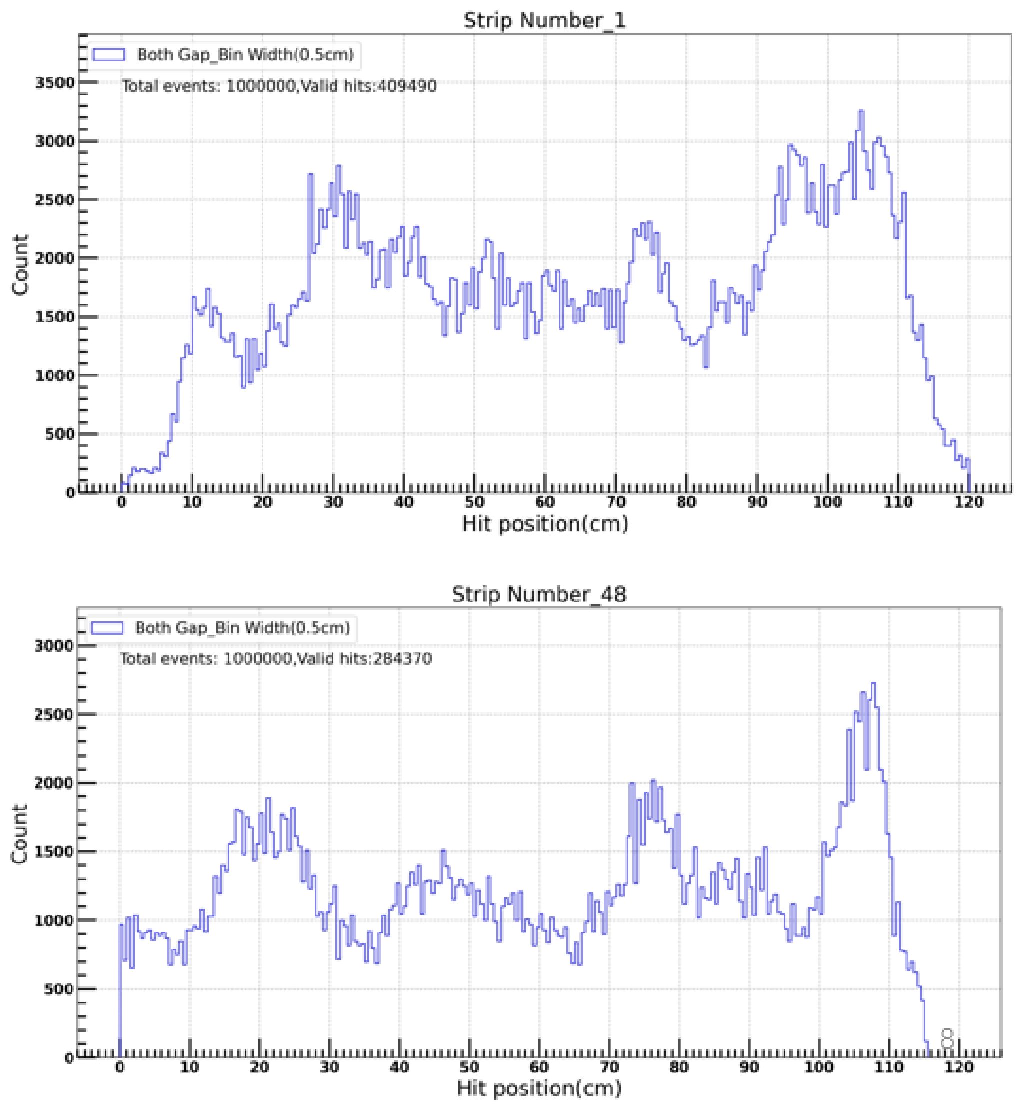


Figure 9: Plots of data analysis for finding the position of spacers for each strip

Also, for measuring with two gaps we expect to see a uniform distribution because the gamma rays can pass through only one gap and we would see the effect, and the plots show a more uniform distribution than for each gap, but there are still some variations in our distributions as it is obvious from Figure 10. The reason for seeing variations in the distributions might be because of the effect of other materials outside of the chamber which are located between the gamma source and the chambers.

In order to see that effect, we put a lead brick in front of our chamber, between the gamma source and chamber, and did the measurement again. The hit map for all the strips is shown in Figure 11 and we can clearly see that the lead break prevented the gamma rays from reaching the detectors.

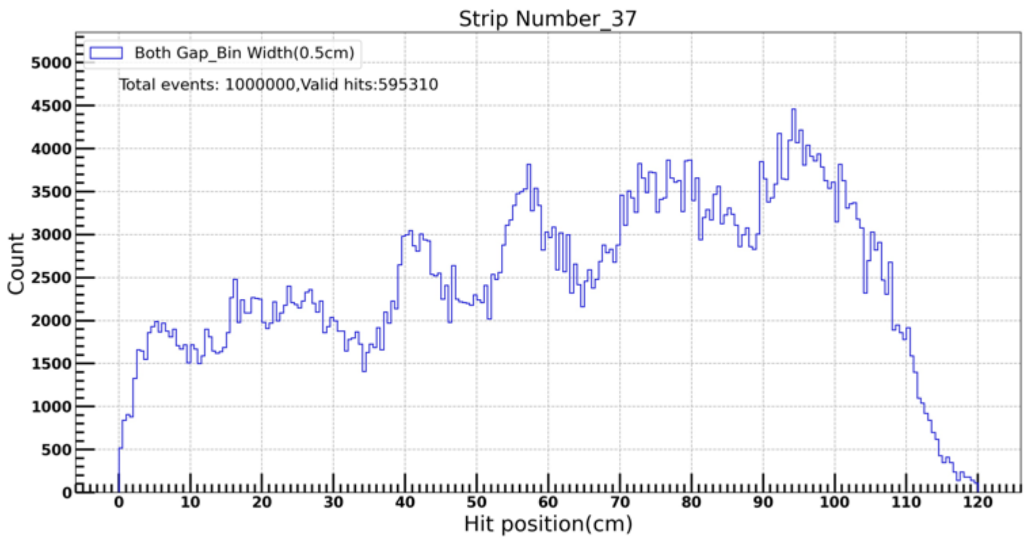


Figure 10: Gamma hit distribution for both gaps

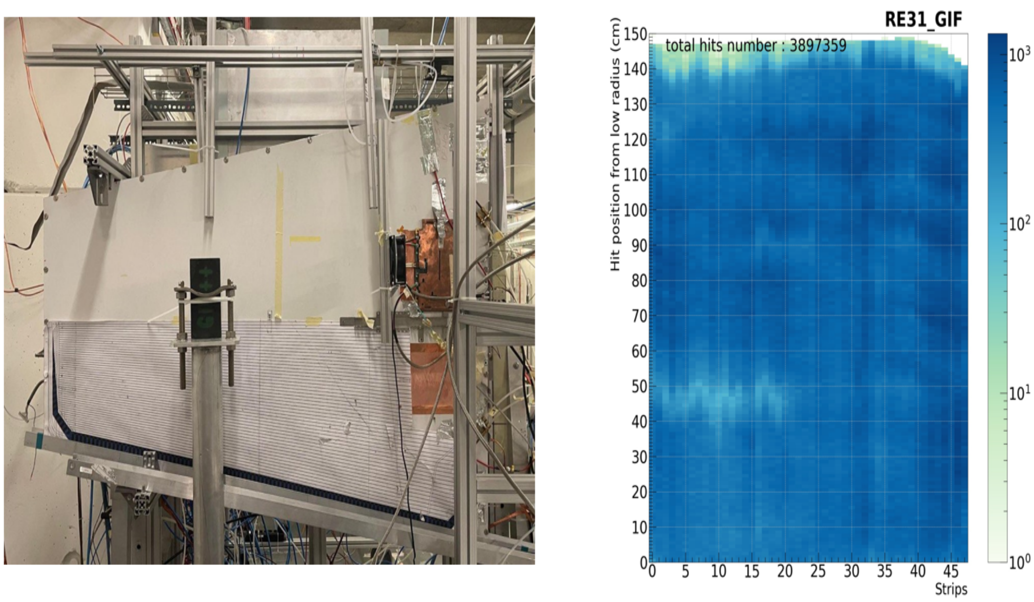


Figure 11: Using a lead brick in order to see the affection in data and plots.

Also, the effect of the brick is clear in the plots for each strip which is shown in Figure 12 that around the hit postition of 40-60 cm, we see a big dip. The lead brick was in front of about half of the strips so its effect is shown only on the first half of the strips. The effect is shown as a dip at almost the same position for the first half of the strips.

Therefore, we can conclude that the materials outside of the chambers can affect our data taking and the efficiency of our chamber, so it is better to have minimum materials between our source and detectors.

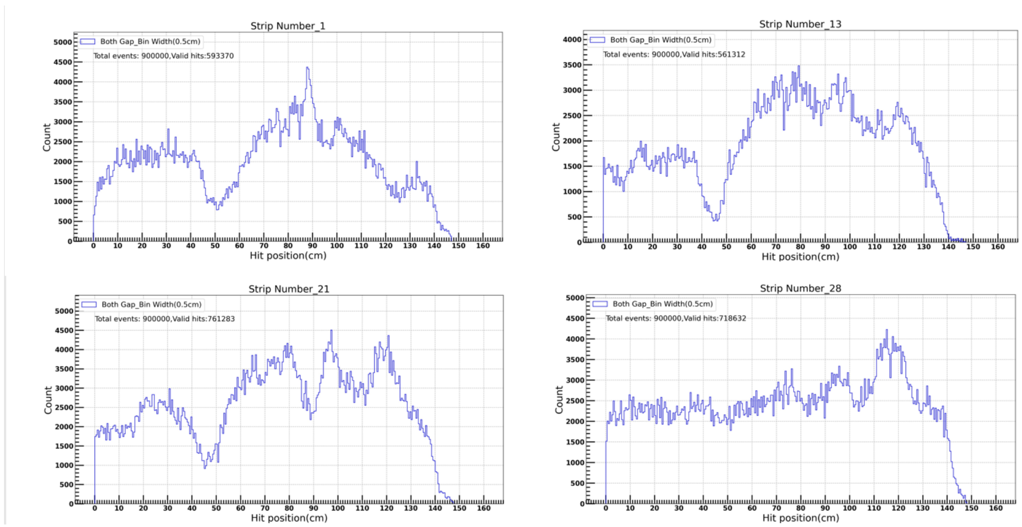


Figure 12: Plots of each strip that are affected and not affected by the lead brick

# 3 Second Project: Efficiency analysis with cosmics

After the assembly of the iRPC detectors, we should test them, determine the efficiency of the chamber, and find the working point. QC (Quality control) level will be applied to full chambers soon after production, in two steps. Assembled chambers will be tested for cooling circuit tightness and front-end board electronics functionality. Then longer test with cosmic rays will be performed to monitor chamber performance (at different High Voltages (HV)). Detailed descriptions on iRPC chamber assembly and quality assurance can be found in Ref. [4].

In order to test the detectors, we have a cosmic setup in building 904 that the cosmic rays are used in order to see the effects on the chamber. In Figure 13 it is shown schematically how the cosmic test and data acquisition works, and how the data is transferred from chambers to the FEB and BEE as it was explained in the introduction section.

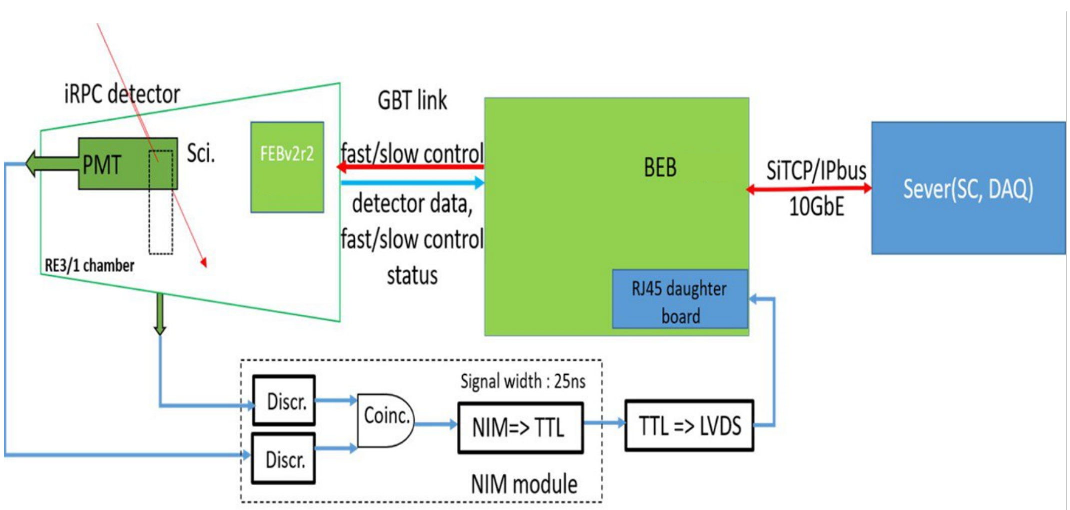


Figure 13: A schematic view of cosmic setup and data acquisition

It is also shown in Figure 14 the setup of the chamber and the scintillators on both sides of the chamber in the laboratory in building 904.

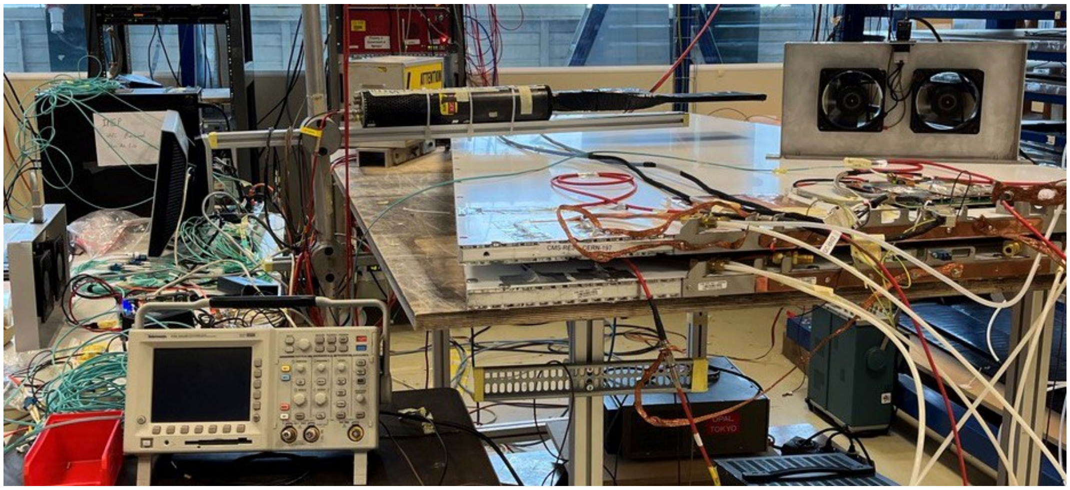

Figure 14: Cosmic setup at building 904

The cosmic setup includes the chamber and two scintillators at the top and the bottom of the chamber. With these two scintillators, we can be assured that a particle has passed through the chamber by seeing the coincidence that happens when we detect an event in both scintillators.

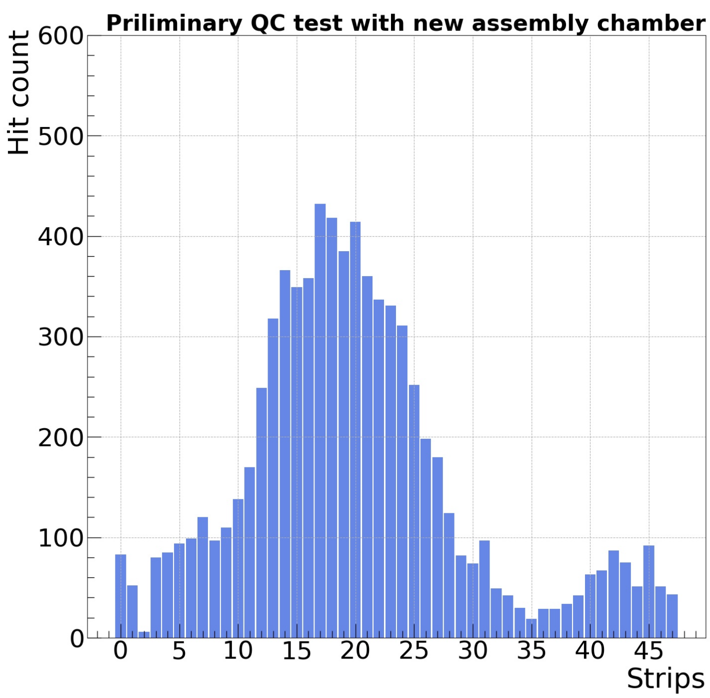


Figure 15: Histogram of the hit count of the events for each strip

We used RE3/1-197 and FEBv2.2 for taking data and this test took about 16 hours. After analyzing the data, we can see in Figure 15 that how many events each strip had been detected.

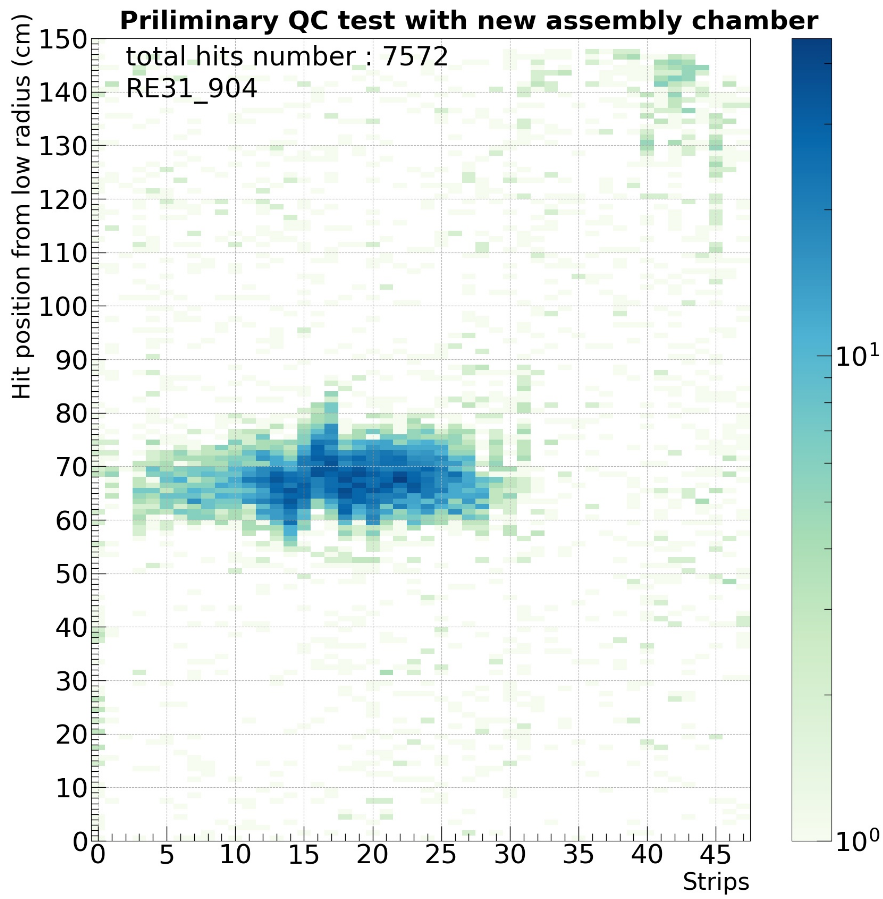


Figure 16: Hit map of the event detected by the half chamber

The efficiency is estimated as the ratio of the number of detected muons to the total number of triggers. The signal arrival time of each of the two ends of the strip should be within a time window associated with the external trigger. This time window depends on the area covered by the scintillators along the strips. We can determine the width of this window by the blue and green spots in the hit map of Figure 16, and we can see the part of the chamber that had detected the events. Therefore, after the determination of the window, we made the efficiency curve as a function of the HV which is shown for the chamber's test in Figure 17.

Also, one of the important parameters which we can determine from the efficiency plot is the Working Point (WP). In order to determine the optimal WP of each prototype, we study their efficiency as a function of the applied effective high voltage. Therefore, HV scans are performed. The goal of the HV scan, as mentioned before, is to study the efficiency as a function of the high voltage for all the iRPC prototypes to find the best working high voltage for every chamber but also to study cluster size associated to the passage of a muon as well as to estimate the noise rate.

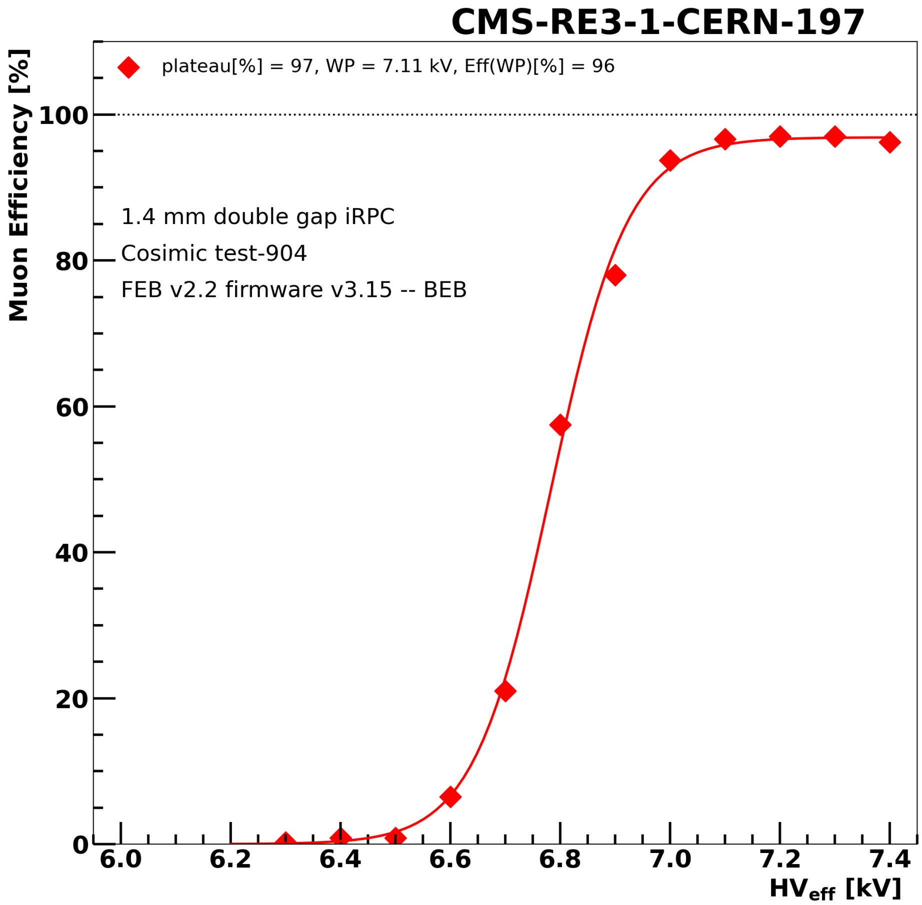


Figure 17: Efficiency curve of QC test of newly assembled chamber

The efficiency curve is usually well described by a sigmoid function:

$$\epsilon = \frac{\epsilon_{\text{max}}}{1 + e^{-\lambda(\text{HV}_{\text{eff}} - \text{HV}_{50})}}. \tag{1}$$

Where $\epsilon$ is the efficiency at a given $\text{HV}_{\text{eff}}$, $\epsilon_{\text{max}}$ is the plateau of this fit function, It is determined by the slope of the fit function at $\text{HV}_{\text{eff}}$ corresponding to 50 percent of the maximal efficiency. This can be expressed by the following formula:

$$\text{slope} = \frac{\text{d}\epsilon}{\text{d}(\text{HV}_{\text{eff}})} = \frac{\lambda\epsilon_{\text{max}}}{4}. \tag{2}$$

To determine the working point, we use the following definition adopted by the CMS collaboration for the 2 mm gas gap RPC:

$$\text{WP} = \text{HV}(50) - \frac{\log(\frac{1}{0.95} - 1)}{\lambda} + 150(\text{V}), \tag{3}$$

and the working point is determined in Figure 17 which is close to 7.1 keV.

## Acknowledgments

The CERN summer program is a great experience for the young people to learn a lot about the cutting-edge science methods, and I was very pleased and honored to take part in this program. I would like to acknowledge Qingfeng Hou and Jianing Song for sharing their expertise and guiding me through my summer student project, supervisor Salvatore Buontempo and all RPC group members for giving me the opportunity to learn new things and be a part of the great community.

## 4 References

1. CMS Collaboration, The Phase-2 Upgrade of the CMS Muon Detectors, CERN-LHCC-2017-012, CMS-TDR-016 (2017)

2. Kou, H., Liu, ZA., Zhao, J. et al. R and D of back-end electronics for improved resistive plate chambers for the phase 2 upgrade of the CMS end-cap muon system. Radiat Detect Technol Methods 6, 306–316 (2022).

3. https://gitlab.cern.ch/cms_ rpc_muons_firmware/feb/feb-v2-firmware

4. L. Pant et al., “Resistive Plate Chambers for the RE4 upgrade of the CMS endcap system”, JINST 7 (2012) P10025, doi:10.1088/1748-0221/7/10/P10025.